Erosion dynamics of a wet granular medium

Gautier Lefebvre[*] and Pierre Jop[†]
Surface du Verre et Interfaces, UMR 125 CNRS/Saint-Gobain, 39, Quai Lucien Lefranc, F-93303 Aubervilliers Cedex, France
(Received 2 July 2013; published 23 September 2013)

Liquid may give strong cohesion properties to a granular medium, and confer a solidlike behavior. We study the erosion of a fixed circular aggregate of wet granular matter subjected to a flow of dry grains inside a half-filled rotating drum. During the rotation, the dry grains flow around the fixed obstacle. We show that its diameter decreases linearly with time for low liquid content, as wet grains are pulled out of the aggregate. This erosion phenomenon is governed by the properties of the liquids. The erosion rate decreases exponentially with the surface tension while it depends on the viscosity to the power -1. We propose a model based on the force fluctuations arising inside the flow, explaining both dependencies: The capillary force acts as a threshold and the viscosity controls the erosion time scale. We also provide experiments using different flowing grains, confirming our model.

DOI: 10.1103/PhysRevE.88.032205 PACS number(s): 81.05.Rm, 68.08.De, 92.40.Gc

I. INTRODUCTION

It is commonly known that the addition of a small amount of liquid in a granular medium brings cohesion properties due to the surface tension of the liquid. Such a mixture may have a strong solidlike behavior [1,2], and, for instance, enables one to build sand castles. The properties and rheology of homogeneous wet granular materials have received much attention from experimental [3,4] and numerical points of view [5,6]. However, the situations encountered in nature or industry often present heterogeneous systems, where the liquid content is not homogeneously distributed over space.

This is the case for some landslides where the basal material is more cohesive than the flowing one. Such a situation arises, for example, because of humidity. To model their dynamics, the evolution of the interface between the erodible ground and the flowing material is still studied experimentally or numerically [7,8] and the effect of the cohesion on erosion remains unknown.

In the industrial context, many processes blend powders and grains with liquids. Understanding the mechanisms of the spreading of the liquid is important to avoid lump formation when preparing dough in the food industry, but also in the granulation phenomenon to obtain pills in the pharmaceutical industry [9], or during the production of slurries for mortar or concrete in building materials [10,11]. During the first stages of the blending, wet areas are in contact with dry flowing grains.

We can expect a morphological evolution of the cohesive medium through exchanges between the two areas. More precisely, in the case of low water content, one may expect erosion of the cohesive phase to occur by extraction of grains from the cohesive medium. Despite the large interest of industry in these processes, the precise mechanisms of these initial steps are not known. What are the exchange rates between these phases?

Although erosion of a granular bed by a liquid flow is well described by transport models [12,13], erosion by a granular flow is not yet as well understood. Nonetheless, attempts to model the effect of the flowing grains on erosion are found in different fields in literature. Erosion of a substrate by a granular phase is of interest for geomorphology, where empirical laws are derived from field observation and from model experiments [14,15]. The erosion rate is usually related to the kinetic energy of impacting grains [15] as in the seminal models of wear production by sand blasting [16,17], where the erosion rate scales with the velocity of impacting grains to a power between 2 and 5 [18]. In the case of enduring contact, fretting wear has been shown to be proportional to the normal load [19]. However, two main points are questionable: First, the stress and flowing conditions at the granular interface are still a matter of debate, especially for dense flows [20], and are hardly linked to the erosion processes [14,21]. What is the driving mechanism for granular erosion? Second, the cohesive media may not be considered as a continuous material since its internal length scale is of the same order of size as the flowing grain. Thus the previous laws derived for brittle or plastic materials showing that the erosion rate decreases with the square of the tensile strength may not apply [22]. We expect on the opposite that forces developed by a stretched capillary bridge [1] will govern the erosion process.

In this paper, we study this erosion phenomenon experimentally with a model system. Here, cohesion is brought by capillary bridges only. The eroding flow is constituted of dry-dense granular matter. We explore the dynamics of erosion in regard to the properties of the liquids in the wet granular medium, and to the properties of the flowing grains. We present a model of erosion that reveals unexpected dependencies and that may be used to better understand the mixing issues mentioned above.

II. EXPERIMENTAL SETUP

A. Materials and device

We used a thin Plexiglas cylinder with an inner diameter of 14.2 cm and a depth of 0.5 cm as a rotating drum (Fig. 1). These dimensions correspond to an aspect ratio of around 28, so the drum can be considered as two dimensional. We introduced wet material, of a controlled liquid content, to form

[*]gautier.lefebvre@saint-gobain.com
[†]pierre.jop@saint-gobain.com; www.svi.cnrs-bellevue.fr/spip

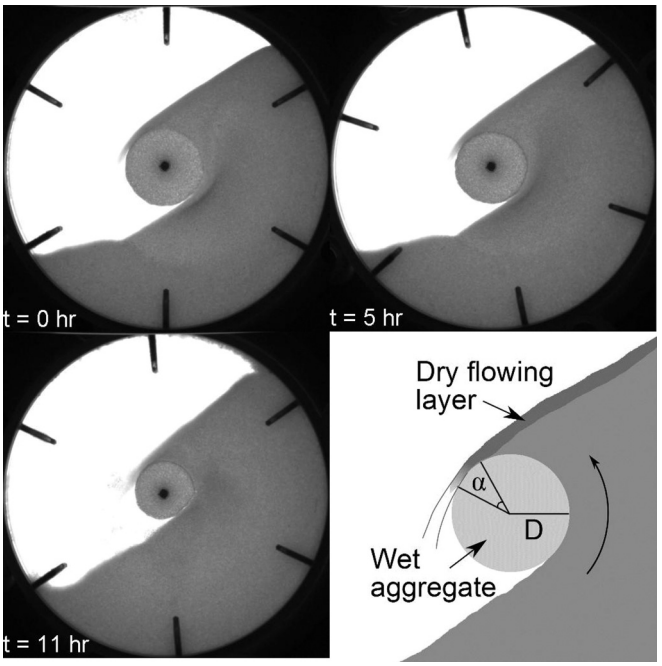

FIG. 1. Images of the drum during the experiment, with glass beads and silicone oil V100. We can see the evolution of the aggregate diameter. The dark spot in the middle of the cylinder is a glued tiny pillar helping to keep the aggregate at the center. On the bottom right is a sketch of the region of interest. D is the diameter of the aggregate. α is the portion submitted to erosion.

a circular aggregate of diameter $D \simeq 3$ cm at the center of the drum. To do so, we first mix an amount of grains and liquid, with the help of a spatula, until we obtain a homogeneous mixture. The cohesion forces that tie the aggregate will also make it stick to the vertical drum walls, and remain at the center. Then, we filled half the left volume with dry grains before closing the drum, and putting it into rotation. Different types of materials have been employed, and are summarized in Table I. Phonolite has an important roughness, and thus is close to real materials. We also used several kinds of beads ranging from 0.2 to 1.3 mm in diameter. We will use different notations for the flowing-grain diameter d and for the radius of wet grains r inside the aggregate. Different liquids were used, water, glycerol, ethylene glycol, and silicone oils, in order to

TABLE I. Granular materials employed in the experiments, and physical properties. The flowing-grain diameter is denoted by d and the radius of grains inside the aggregate is denoted by r.

Granular material	Density ρ (g/cm^3)	Size d (mm)
Phonolite grains	2.6	0.8–1
Glass beads (GB)	2.5	0.2–0.4
		0.5
		0.8–1
		1–1.3
Polystyrene beads (PS)	1	0.5
Zirconium silicate beads	3.8	0.5
Zirconium oxide beads	5.5	0.5
Stainless steel beads	7.9	0.5

TABLE II. Liquids employed in the experiments, and the measured physical properties.

Liquids	Viscosity (mPa s)	Surface tension (mN/m)	Contact angle
Water	1.0	72	32
Silicone oils V10–V10000	10–10 000	21	<5
Water-glycerol	1.3–560	60–72	30–46
Water-ethylene glycol	10–17	48–49	31

vary the surface tension γ, from 20 to 70 mN/m, and viscosity η, from 1 to 10^4 mPa s. These liquids are listed in Table II.

For the range of measured surface tension γ, the typical granular Bond number is always high, with $\mathrm{Bo}_g = 2\pi\gamma r/mg > 50$, where r is the wet grain radius and m the mass of the grain. That is why cohesion from capillary bridges here can easily overcome the gravity. The aggregate then has enough cohesion to sustain itself, and not break under its own weight. The capillary length $l_c = \sqrt{\gamma/\rho_{\mathrm{liq}}g}$ is around 2.6 mm for water, much larger than the typical size of capillary bridges, so gravity will not deform them. Finally, drainage is limited by viscous effects, as the liquid should travel through thin films of liquids, whose thickness is the roughness of the bead surface δ. Considering the hydrostatic pressure on the size of the aggregate, we obtain a drainage time on a distance r of $t_{\mathrm{drain}} = \eta D/\delta^2\rho_{\mathrm{liq}}g \simeq 10^4$ s for $\eta = 10$ mPa s. This means that gravity-driven drainage effects are prevented, as the rotation period is much smaller than this time.

B. Measurements

During the rotation, snapshots are regularly taken, and the relevant information is retrieved by image analysis. The dry grains and the flow can be identified from grayscale levels, and the shape of the aggregate can be followed during the experiment. The lateral view of the drum of Fig. 1 shows how the flow is modified by the aggregate. Most of the grains flow above it, but a small part of them can pass under. Meanwhile, the moisture and temperature of the room are recorded in the process. Temperature is needed for a precise determination of the liquid properties, such as viscosity. Humidity is a source of liquid in the granular medium, as shown by Bocquet *et al.* in Ref. [23], which can influence the results. However, we checked that the influence of this parameter is weak compared to our data dispersion.

For experiments with glass beads, the progressive liquid spreading due to erosion in the dry area can alter the flow properties. Cohesion appears in the surrounding medium until it sticks to the edges of the drum. The setting is then widely modified, so we use only the first part of the experiment, when the spreading of the liquid is still low enough.

III. EXPERIMENTAL RESULTS

A. Multiple regimes

Trials have first been led with phonolite and water, for different liquid contents. In the following, we choose to use W, the ratio of liquid volume on the total volume of aggregate.

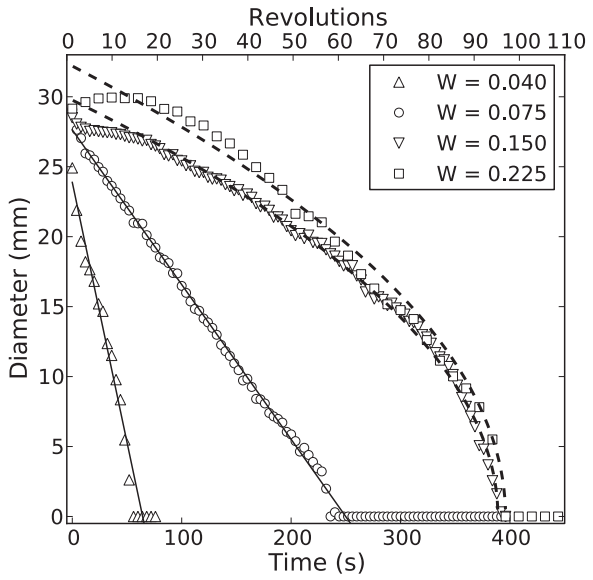

FIG. 2. Time evolution of the aggregate's diameter, with phonolite grains, for different water contents. The upper axis is the number of revolutions of the drum. Solid lines are linear fits, and dashed lines are square root function fits.

As there is no compaction of the aggregates in our experiments, W is not changed without the addition or withdrawal of liquid. We had to use quite high levels of liquid contents due to the high roughness of phonolithe grains, between 4% and 22.5%. The rotation speed was maintained at 0.349 rad/s, corresponding to an 18 s period. Figure 2 shows the variation of the aggregate diameter, from its initial value to zero, when it disappears in the flow. The lifetime of the aggregate (a few minutes) increases with W. For low liquid contents, the diameter decreases linearly with time. Such behavior can be easily justified by simple assumptions. In this case, capillary bridges are individual, so the behavior of interfacial grains does not depend on the other grains farther below the surface. The erosion of the grains is then a local mechanism. Moreover, the flow properties are stationary, thus we assume that the mechanical action of the flow is constant with time. Since the wet aggregate is assumed to be homogeneous, the local erosion rate should also be constant with time. Finally, the diminution of the aggregate area should scale with the portion $\alpha D/2$ of the perimeter undergoing the erosion (Fig. 1), leading to $-\frac{d(\pi D^2)}{dt} \propto \alpha D$. We assume that the angle α depends on the geometry only, and remains unchanged. The diameter decrease would then be linear: $\frac{dD}{dt} = cst$.

For the higher liquid contents, we have a slower evolution, and even a growth phase for $W = 22.5\%$. This growth is probably enabled by the rearrangement of the liquid distribution. If the liquid network is sufficiently connected, suction may bring the liquid to the edge of the aggregate and create new capillary bridges, with initially dry grains, coming from the flow. We saw that gravity-driven drainage was not permitted because of viscous effects. Moreover, when the liquid content is high enough, the liquid is no longer distributed into single capillary bridges. The Laplace pressure may be weaker in water pockets, implying more than two grains, and on the opposite, it will play fully on the newly formed bridge. That is why liquid transport may occur here, as it is driven by capillary effects, which are stronger than gravity at the grain scale. The diameter seems to follow a square root collapse with time (Fig. 2). As a simple tentative explanation, we can consider that the flowing grains pump the liquid toward the surface of the aggregate, thus the erosion will be lower at the beginning while the degree of saturation in the core decreases. Then, the erosion rate increases when the diameter decreases, as the water content is lower inside. We reserve this issue for future work.

The linear regime appears then as a simpler process, which does not involve liquid migration inside the aggregate. In this regime, we can measure an erosion rate E from the slope of the lines to quantify the speed of the process. We define E as a dimensionless parameter by rescaling the aggregate diameter D by the bead diameter d, and the time by the rotation period of the drum T:

$$\frac{D - D_0}{d} = -E\frac{t}{T}. \quad (1)$$

E is then a positive number, counting the number of layers of grains eroded from the surface of the aggregate, for each revolution of the drum.

B. Liquid properties

In the following, we use a relatively low liquid contents to remain in the linear regime of erosion for which we can measure an erosion rate. The typical value will be $W = 0.3\%$, and otherwise precised. Figure 3 shows a typical run of the experiment. The diameter of the aggregate decreases linearly, and the fit provides a value of erosion rate E as defined in Eq. (1).

To stretch a capillary bridge linking two grains, one must overcome two forces, one coming from the surface tension and the other one from the viscosity of the liquid. The forces

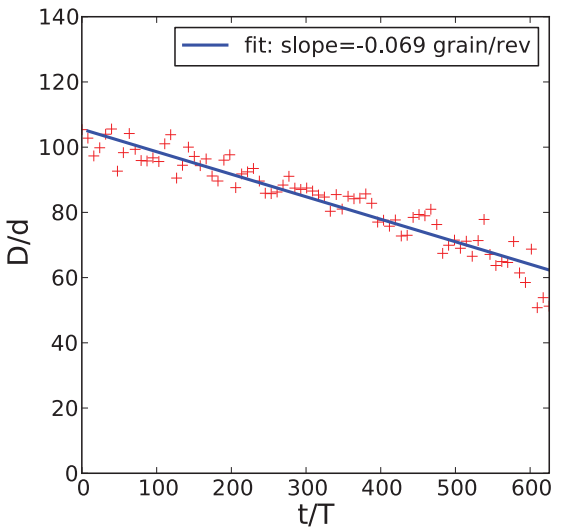

FIG. 3. (Color online) Linear decrease of the aggregate diameter with 200–400 μm glass beads, for $W = 0.3\%$. The liquid used is silicone oil V100.

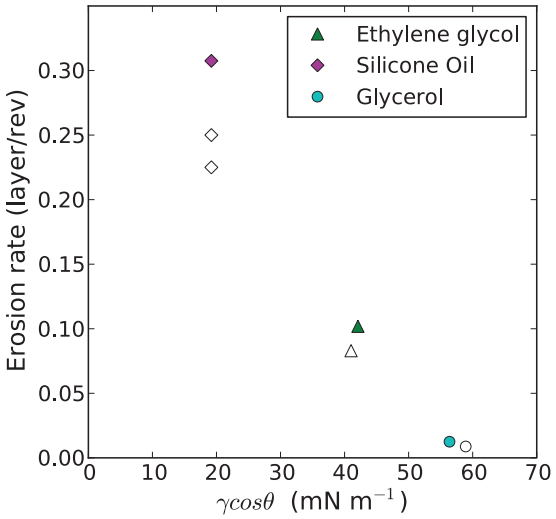

FIG. 4. (Color online) Erosion rate vs $\gamma \cos\theta$ for different liquids and glass beads. For solid symbols the viscosity is around 10 mPa s, and for open ones it is around 20 mPa s.

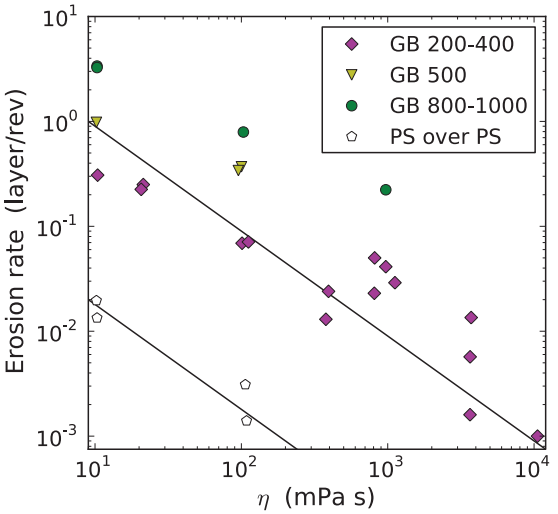

FIG. 5. (Color online) Erosion rate vs viscosity for different beads. The surface tension is around 21 mN/m. In each case, we made the aggregate with the same 200–400 μm glass beads, except for the polystyrene bead trial, where we used polystyrene beads for both the flow and the aggregate. The lines of slope -1 show a trend. Typical error bars estimated from error measurements are smaller than the markers. However, experiments with a similar viscosity display some variability.

developed by a capillary bridge are approximated by [1]

$$F_{\text{cap}} = 2\pi\gamma r\cos\theta, \quad F_{\text{visc}} = \frac{3}{2}\pi r^2\eta\frac{1}{s}\frac{ds}{dt}, \tag{2}$$

θ being the contact angle, and s the separation distance between the two beads. These are first order approximations regarding s. Only the normal viscous dissipation is considered, and we assume that most of the viscous dissipation arises from normal displacement. We expect then for both surface tension and viscosity to increase the resistance to erosion, and thus to observe lower erosion rates when they increase. In order to observe the effect, another set of experiments has been carried out with various liquids. We used the same protocol as previously, with a 24 s period. The liquid content is fixed at $W = 0.3\%$ or otherwise precised. Figure 4 shows the evolution of the erosion rate with the surface tension. The different liquids have a similar viscosity, from 10 to 20 mPa s. The erosion rate strongly decreases even for a small range of surface tension.

Silicone oils allowed us to explore the influence of viscosity from 10 to 10 000 mPa s (V10–V10000), and have a conveniently constant surface tension of 21 mN/m. Figure 5 plots the erosion rate versus the viscosity. The decrease of the erosion rate spreads over three decades, and a similar trend is observed for other trials with other glass beads and polystyrene beads. The lines of slope of -1 in log-log scales on this plot show a trend in agreement with the results, even if we observe a slightly lower slope for the bigger glass beads.

In the previously defined linear erosion regime, the liquid content still has an influence on the erosion dynamics. Figure 6 shows the erosion rate measured for different liquid contents ($W = 0.3\%$–1.5%), with two different liquids. In this range, we have enough liquid to cover the surface of the beads by a layer of liquid. Meanwhile, we are still below a threshold of coalescence of capillary bridges, and they are formed only between pairs of beads. Moreover, for a homogeneous distribution the liquid network is well described in Ref. [1], from which come the results and relations of this section we rely on. The cohesion forces have simple expressions [Eq. (2)], and it is noticeable that these two cohesion forces do not depend on the volume of the bridges in first approximation. The influence of the liquid content may be explained as follows. Under the assumption of a homogeneous distribution of liquid, a further addition of liquid will increase the bridge volume V. If we assume all the liquid to go into the capillary bridges, V is linked to the liquid content by $\tilde{V} = \frac{8\pi W}{3\rho N}$, V being rescaled by r^3, where N is the average number of bridges per bead. Therefore the rupture length s_c also increases as follows: $\tilde{s_c} = (1+\theta/2)(\tilde{V}^{1/3} + 0.1\tilde{V}^{2/3})$ [24]. $\tilde{s_c}$ is simply s_c/r. The

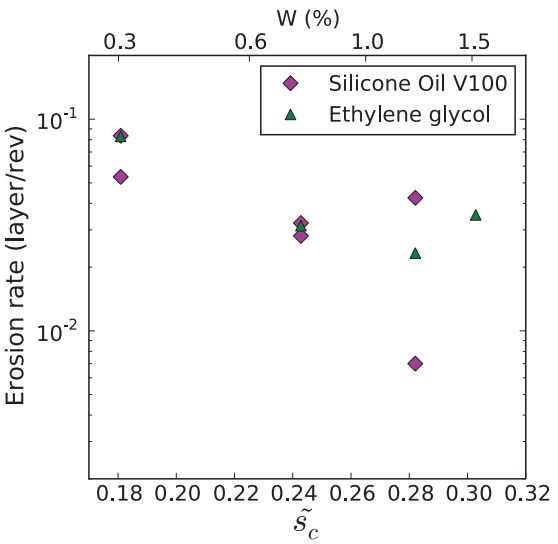

FIG. 6. (Color online) Erosion rate plotted vs the dimensionless rupture length of the capillary bridge. We observe a similar evolution with two liquids of different viscosity and surface tension.

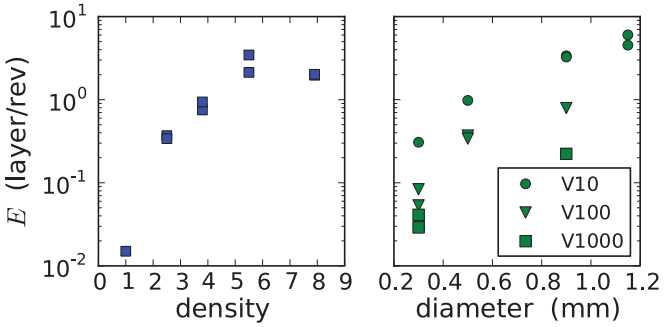

FIG. 7. (Color online) Evolution of the erosion rate with the main characteristics of flow beads. On the left are the variations with the density of mass, using 100 mPa s silicone oil and 500 μm beads of different materials listed in Table I. The variations with the bead diameter are plotted on the right, using glass beads and 10, 100, and 1000 mPa s silicone oils.

rupture length will then contribute to the effective resistance to erosion, but more importantly, the addition of liquid also increases the connectivity of the capillary bridge network. N is experimentally given by $N = 6(1 + \tilde{s_c})$. $\tilde{s_c}$, scaling roughly with $W^{\frac{1}{3}}$ (through $\tilde{V}$), appears as the relevant parameter to analyze the influence of the liquid content. The equations giving $\tilde{V}$ and $\tilde{s_c}$ are solved iteratively to obtain $\tilde{s_c}$ as a function of W.

C. Bead properties

The different sets of beads used also give information about the influence of flowing beads on the erosion dynamics. Here, only the beads of the flow are changed, and the aggregate is always made with 200–400 μm glass beads. This way, the cohesion of the aggregate remains unchanged, and we can independently observe the influence of the action of the flow on the process. We changed two parameters with great consequences on the erosion rate: bead size and bead density.

Figure 7 shows a strong increase of the erosion rate of several decades, with only moderate changes in the mass density and diameter. The scaling appears as clearly faster than a simple proportionality.

IV. MODELING

A. Assessment of the interactions involved

In order to understand how the liquid properties impact the erosion dynamics, we need to evaluate the order of magnitude of the different forces. Since the erosion of the aggregate is a very slow process compared to the dynamics of the flowing grains, we can assume first that wet grains are extracted one by one from the aggregate and, second, that the dry-grain flow is not modified by this mechanism. For this purpose, we introduce a typical velocity, $v \sim \sqrt{gd}$, which scales as the average velocity of the first layer of beads flowing on the aggregate. We explore a wide range of viscosity, hence the Stokes number $\mathrm{St} = mv/\eta d^2$ as defined in Ref. [9], with m the mass of the beads, varies from 10^{-3} to 10, which means that the inertia of the beads can be important for the low viscosities. The capillary number was also varied in a wide range, $\mathrm{Ca} = \eta v/\gamma \sim 10^{-4}$–1. The velocity used is relevant only if the grains are extracted at the same speed as the flowing grains, but this is a questionable point. Using a few fast-camera acquisitions, we measured a typical velocity around 3 mm/s, which is only a tenth of $\sqrt{gd}$. These measures indicate potentially a lower capillary number, and therefore that viscous forces are negligible versus capillary effects. This question will be precised later.

Finally, we can evaluate the typical force $\bar{F}$ undergone by the grains submitted to the flow. We can either choose the stress from gravity $\tau_g = \rho g h \mu$, where h and ρ are the height and the average density of the flowing layer and μ is the friction coefficient at its bottom, or the one from Bagnold's collisional-stress scaling, $\tau_B \propto \rho d^2 \dot{\gamma}^2$, with $\dot{\gamma}$ the shear rate in the flow. The shear rate in the rotating drum geometry is given by $\dot{\gamma} = \frac{1}{2}\sqrt{g/d}$ [25], so we obtain that the stress driving the erosion should scale either as

$$\tau_B \propto \rho g d \tag{3}$$

or

$$\tau_g \propto \rho g h \mu. \tag{4}$$

The former scaling (3) has been confirmed by numerical simulations at the front of a bidisperse granular flow: Yohannes *et al.* in Ref. [26] found an average boundary stress scaling linearly with the bead size, as in Eq. (3). Then, in both cases, the density of the beads impacts directly the boundary stress. Erosion models derived from Ref. [19] suggest that $E \propto \tau$. However, we can notice that a simple proportionality between the erosion rate and ρ or d could not explain the important effect on the erosion rate we observed in Fig. 7. This dependency would be too weak compared to the one we measured. Then either we do not have a simple scaling of the erosion rate, or the average shear stress is not a relevant parameter in the process. The average force $\bar{F}$ can be evaluated with the average shear stress [Eqs. (3) or (4)] on one bead, $\bar{F} = \tau \pi r^2$, leading to a range of force between $\bar{F} \simeq 5 \times 10^{-7}$ N for the Bagnold stress and 2.5×10^{-6} N for the gravity force. We can use the Shield number Θ comparing the tangential and confining forces, usually defined for river bed erosion [13]. Here $\Theta = \bar{F}/F_{\mathrm{cap}}$, as the dominant confining force is F_{cap}. We find that Θ spans from 0.005 up to 0.12 depending on the chosen stress and on the surface tension. The shear force values are then at least ten times less than the capillary forces. This comparison means that erosion is not possible to occur as a simple stretching of the bonds by the average stress.

B. Stochastic approach

Even if the average force undergone by the aggregate's grains is weak compared to the capillary forces, physical quantities are known to have large fluctuations around their average values in a granular medium. Such fluctuations in the granular flow can overcome the cohesion of the aggregate.

1. Shear stress distribution

Only larger values present in the force distribution $P(f)$ are able to overcome the threshold, allowing the stretching of the bonds, until we reach the rupture. Then, in order to build an erosion rate, we need the time for a bridge to reach the rupture, for each level of stress. F_{cap} is the static force, which

defines the lower level of erosion resistance, as the viscous force arises only with stretching speed. We consider that only forces f greater than F_{cap} will contribute to the erosion, at a rate $1/t_{\text{rupt}}$, and with a probability of occurrence $P(f)df$. Under such a hypothesis, the erosion rate derived from this stochastic model should follow

$$E_s = \frac{\alpha T}{2\pi} \int_{F_{\text{cap}}}^{\infty} \frac{1}{t_{\text{rupt}}(f)} P(f) df. \tag{5}$$

We call E_s the theoretical erosion rate derived from this stochastic model. $\frac{\alpha}{2\pi}$ simply represents the portion of the aggregate undergoing the stress of the flow, and we have a dimensionless erosion rate multiplying by T. Writing this model, we assume that the rupture time is lower than the correlation time of the forces. Gardel *et al*. report a correlation time of 10 ms in a hopper for 3 mm beads [27]. We will comment about this assumption below. The fluctuations are typically exponential in a granular material. We chose to use the distribution derived from the q model, verified for static pile [28] and for flow under shear as well [29]:

$$P(f) = \frac{f^2}{2F_0^3} e^{\frac{-f}{F_0}}, \tag{6}$$

F_0 being linked to the average force of the distribution by $\bar{F} = 3F_0$. Regardless of the precise distribution, the exponential decrease for high forces is a generic feature for a granular medium in a wide variety of conditions [30,31]. This approach brings us back to the previous issue of the velocity of extracted grains: Different levels of forces lead to different rupture times, thus to various extraction velocities. From this we need to evaluate the rupture time relations with the liquid properties as well as the stress level.

2. Capillary bridge dynamics

Evaluating the rupture time requires studying the bridge dynamics. Initially, the main force acting on the bridge is the capillary force. Then, as the bond is stretched, viscous forces will arise. We use a simple equation to model the bridge dynamics:

$$m\frac{d^2s}{dt^2} = f - 2\pi\gamma r\cos\theta - \frac{3}{2}\pi r^2\eta\frac{1}{s}\frac{ds}{dt}. \tag{7}$$

We consider here a single capillary bridge, submitted to a constant traction force f. Here we use first order expressions of the forces, the capillary forces, for instance, which actually depend on the separation distance [1]. We consider two different limits cases of this nonlinear differential equation (7). First, for low viscosity, inertia will dominate compared to the viscous force. Neglecting this term, we can then integrate from the contact distance δ, due to roughness, to the rupture length:

$$t_{\text{rupt-inert}} = \sqrt{\frac{2mr\tilde{s_c}}{f - 2\pi\gamma r\cos\theta}}. \tag{8}$$

If viscosity is high enough, then inertia is negligible, and again we can easily integrate without the left-hand side to obtain the rupture time:

$$t_{\text{rupt-visc}} = \frac{\frac{3}{2}\pi\eta r^2 \ln\frac{s_c}{\delta}}{f - 2\pi\gamma r\cos\theta}. \tag{9}$$

We evaluate these time scales for a traction force f being twice the capillary force: We find values around 0.1 ms for the inertial time, and from 0.3 to 300 ms for the viscous time. Comparing to the correlation time of forces from literature, the most viscous case and the lower levels of forces will not verify the assumption we made. Still, very large forces can achieve the rupture of the bridge in a short enough time. To push further the analytical development of the model, now we make the assumption that the sum of the two characteristic times provides a good approximation of the actual rupture time.

3. Erosion rate

Using the force distribution (6) and the total rupture time (8) and (9), the erosion rate can then be developed in the following form:

$$E_s = \frac{\alpha T}{4\pi F_0^3} \int_{F_{\text{cap}}}^{\infty} \frac{f^2 e^{\frac{-f}{F_0}}}{\frac{a}{\sqrt{f-F_{\text{cap}}}} + \frac{b}{f-F_{\text{cap}}}} df, \tag{10}$$

with $a = \sqrt{2mr\tilde{s_c}}$ and $b = N_c\frac{3}{2}\pi\eta r^2\ln\frac{s_c}{\delta}$, constant coefficients depending on the bead and liquid properties. We have to consider the multiplicity of capillary bridges through the number N_c, which is now present both in the viscous force (in b) and in the capillary force F_{cap}, even if we keep the same notation. The effective number of capillary bridges per bead in the aggregate can be reduced next to the walls. On the other hand, we do not consider the friction caused by the sidewalls, which can increase the resistance to erosion of the aggregate. But in the end this concerns only a small fraction of the grains, around 10%, as we have 20 layers of grains in the width of the drum. For the beads submitted to erosion, at the surface of the aggregate, we consider this number of bonds to be reduced to half: $N_c = N/2 = 3(1+\tilde{s_c})$. The substitution $u = \frac{f-F_{\text{cap}}}{F_0}$ underlines the main physical trends in the expression

$$E_s = \frac{\alpha T}{6\pi^2} \frac{F_{\text{cap}}^2}{F_0\eta N_c r^2 \ln\frac{s_c}{\delta}} e^{-\frac{F_{\text{cap}}}{F_0}} I\left(\frac{F_0}{F_{\text{cap}}}, \frac{a}{b}\sqrt{F_0}\right), \tag{11}$$

with

$$I\left(\frac{F_0}{F_{\text{cap}}}, \frac{a}{b}\sqrt{F_0}\right) = \int_0^{\infty} \frac{u\left(1+\frac{F_0}{F_{\text{cap}}}u\right)^2}{1+\frac{a}{b}\sqrt{F_0 u}} e^{-u} du. \tag{12}$$

The first result of this model is the main dependencies of the erosion rate: It decreases exponentially with the capillary force, and scales as η^{-1}, as we observed in Fig. 5. The dimensionless integral I varies with dimensionless numbers as well, $\frac{F_0}{F_{\text{cap}}}$, which is $\frac{3}{N_c}\Theta$, and $\frac{a}{b}\sqrt{F_0}$. The second one can actually be written as a combination of the first one, and other usual numbers: $\frac{a}{b}\sqrt{F_0} \propto \Theta\sqrt{\text{St}/\text{Ca}}$. These numbers are rather small for the set of parameters used in most experiments. Then I is close to its limit 1, and will give a weaker influence on the erosion rate with the physical parameters. It is worth noting that we do not expect this stochastic erosion rate to exactly match the experimental data. Indeed, the roughness of the

surface or the local variations of the number of bridges that would delay the erosion are not taken into account.

In a different limit of $\Theta \gg 1$ and $\Theta\sqrt{\mathrm{St}/\mathrm{Ca}} \ll 1$, the viscous rupture time would dominate, and we obtain a different expression for the erosion rate:

$$E_s = \frac{\alpha T}{2\pi} \int_{F_{\mathrm{cap}}}^{\infty} \frac{f}{b} P(f) df \simeq \frac{\alpha T}{2\pi b} \bar{F}. \qquad (13)$$

Then, the erosion rate is proportional to the average force, according to the wear models described in Ref. [19]. In the following, we confront our model with the experimental data in more detail.

V. ANALYSIS AND DISCUSSION

A. Influence of liquid properties

Plotting the erosion rate times $\frac{\eta N_c r^2}{F_{\mathrm{cap}}^2} \ln \frac{s_c}{\delta}$ (Fig. 8) allows us to represent liquids of different physical properties on the same graph, and should exhibit an exponential decrease with F_{cap}, neglecting the variations of I. The points are well gathered on the same line in log-lin scales, except for the experiments with water. This shift is probably due to evaporation during the experiment, reducing the effective liquid content in the aggregate. An evaporation test showed that half the initial water content in the aggregate disappeared after 40 min, which was the time of measurement for this experiment. Similar tests on the other liquids showed no effect of evaporation. The scaling with η^{-1} of the erosion rate is also confirmed by this plot. The fit provides an evaluation of the parameter F_0, related to the average force $\bar{F}$. We found $\bar{F} = 5.7 \times 10^{-5}$ N for the standard setup of our experiments, that is, glass beads of 200–400 μm diameter. Nevertheless, it is straightforward to integrate numerically Eq. (5), and fit $\bar{F}$ by successive iterations: We find $\bar{F} = 7.3 \times 10^{-5}$ N. As this value is close to the previous one, the first order of the variations is well captured by the first parts of Eq. (11), meaning that the integral I [Eq. (12)] has a moderate variation.

However, this value is quite different from the force estimation based on dimension analysis [Eqs. (3) and (4)], but it is still less than the capillary force, whose comparison justifies our stochastic approach. An explanation would be that the surface of the aggregate is not flat and that the highest wet grains experience larger forces, leading to a faster erosion of those grains. Another tentative explanation is to consider capillary bridges to break one by one, decreasing by a factor $3(1 + \tilde{s}_c)$ the cohesive force and the fitted $\bar{F}$. In both cases, the erosion rate is expected to increase and to lead to an overestimation of the mean force $\bar{F}$. Moreover, the fitted value of $\bar{F}$ is sensitive to the precise distribution function $P(f)$, which still remains subject to research. Nevertheless, the exponential decrease arising from the distribution tail is a strong result unrelated to the value of $\bar{F}$. In the next section, we test our model with the scaling of the exerted force by the flow.

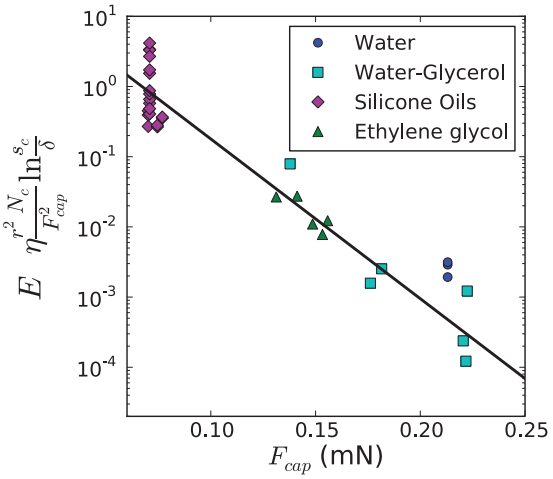

FIG. 8. (Color online) Exponential decrease of the erosion rate with the capillary force. Experiments realized with 200–400 μm glass beads. The line is an exponential fit of the data.

B. Influence of flow properties

The exponential decrease with the capillary force confirms an important point of this model, which is the role of stochastic fluctuations in the erosion process. Now as we dispose of a data set where only the average stress is varied, we can confront the results with the model predictions. As the aggregate is prepared likewise for each set, using glass beads, there is no change in capillary force or in the viscous term in Eq. (11). However, the average force, and therefore F_0, will change with ρ and d according to Eq. (3).

Figure 9 shows the exponential decrease of $\rho * E$ vs $1/\rho$ and similar variations on the bead size. This is the expected dependency with the average force according to Eq. (11). As in the previous part, we integrate I and fit by iterations until we obtain an evaluation of the average force $\bar{F}$. We convert the result to the equivalent value for the standard flow setup (200–400 μm glass beads), according to Eq. (3). The data set on the mass density gives a value of 5.4×10^{-5} N, and the set on the diameter with silicone oil V10 gives 5.1×10^{-5} N, which are fairly concordant, and still quite close to the previous one, using the capillary force variations. This exponential decrease with the dimensionless number F_{cap}/F_0 is confirmed on the two independent parameters, by separate experiments, and supports the relevance of considering stress fluctuations

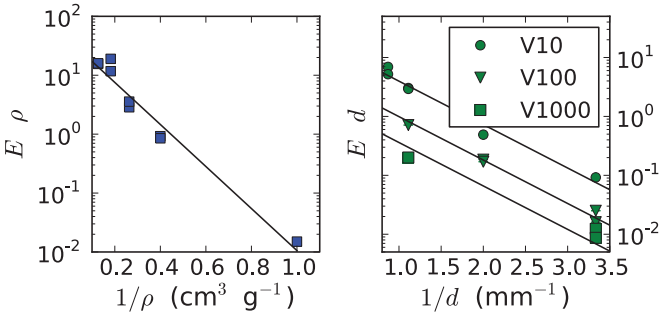

FIG. 9. (Color online) Exponential decrease of the erosion rate with the scaling parameter of the average force, according to the model developed above. On the left are the variations with the density of mass and a fit, and on the right with the bead diameter. On the right plot the V10 set is fitted, and the line reported seems also in good agreement with the two other sets.

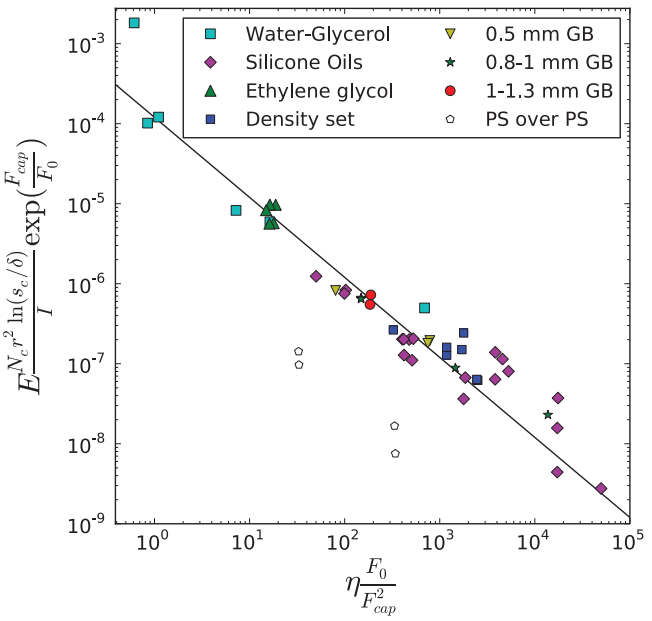

FIG. 10. (Color online) Master curve with all experimental results, enlightening the scaling of the viscosity, extended to the different setups. The results with the same x position in a given set of data show the variability in the erosion rate.

in the erosion process. This result also confirms the use of the inertial stress for the scaling of the force.

The different sets of results of this erosion experiment show a good agreement with the stochastic model proposed here. The influence on the erosion rate of the physical properties of the liquids involved (viscosity, surface tension, liquid content), and the beads (density, size) has been verified separately, and leads to a concordant evaluation of the fitting parameter $\bar{F}$. Using the right scaling, we plot all the results in Fig. 10, showing that the erosion rates gather on a single master curve. The white symbols in this figure correspond to the polystyrene beads flowing around a polystyrene bead aggregate. They are far below the master curve while the erosion of the polystyrene beads flowing on a glass bead aggregate is well captured by our model (one of the darker blue squares). This is even more surprising as glass beads seem to be eroded faster than polystyrene ones. We do not know the origin of this behavior, and we suppose that arising static electric charges may prevent effective contacts between the beads, reducing the erosion rate. Finally, the slope of the fitted master curve value is $\bar{F} = 7.1 \times 10^{-5}$ N.

VI. CONCLUSION

We measured the evolution of the erosion rate of a wet aggregate with respect to the liquid and grain properties. We showed an unexpectedly strong influence of the surface tension. This effect is captured by the stochastic model we proposed, which shows a good agreement with the different sets of experimental results. We cannot separate the domain of influence of the viscosity and surface tension due to their different roles in the erosion mechanism: We have shown that in conditions of low Stokes number, the viscosity drives mostly the rupture time of the capillary bridge. Meanwhile, surface tension acts as a simple threshold and a shift for the efficient contribution in the stress distribution of the surrounding flow. In the case of a low level of stress, the fluctuations of the flow appear as crucial in the description of the erosion phenomenon. This role of fluctuations has already been pointed out for other interface behaviors, expressed as boundary conditions in Ref. [32]. Fluctuations act also as the triggering effect of quasistatic flows in the work of Pouliquen *et al*. [33], similarly to our experiments, and have recently shown their relevance in impact dynamics in granular media [34].

ACKNOWLEDGMENTS

We thank F. Chevoir for enlightening advises. We acknowledge also P. Raux and C. Clanet for fruitful discussions on the different erosion regimes and E. Gouillart for useful comments on the manuscript.

[1] S. Herminghaus, Adv. Phys. **54**, 221 (2005).
[2] N. Mitarai and F. Nori, Adv. Phys. **55**, 1 (2006).
[3] S. M. Iveson, J. A. Beathe, and N. W. Page, Powder Technol. **127**, 149 (2002).
[4] P. C. F. Møller and D. Bonn, Europhys. Lett. **80**, 38002 (2007).
[5] P. G. Rognon, J.-N. Roux, D. Wolf, M. Naa, and F. Chevoir, Europhys. Lett. **74**, 644 (2006).
[6] V. Richefeu, M. S. El Youssoufi, and F. Radjai, Phys. Rev. E **73**, 051304 (2006).
[7] A. Mangeney, O. Roche, O. Hungr, N. Mangold, G. Faccanoni, and A. Lucas, J. Geophys. Res. **115**, F03040 (2010).
[8] R. M. Iverson, J. Geophys. Res. **117**, F03006 (2012).
[9] B. J. Ennis, G. Tardos, and R. Pfeffer, Powder Technol. **65**, 257 (1991).
[10] B. Cazacliu and N. Roquet, Cement Concrete Res. **39**, 182 (2009).
[11] R. Collet, D. Oulahna, A. De Ryck, P. H. Jezequel, and M. Martin, Powder Technol. **208**, 367 (2011).
[12] E. Lajeunesse, L. Malverti, and F. Charru, J. Geophys. Res **115**, F04001 (2010).
[13] F. Charru, H. Mouilleron, and O. Eiff, J. Fluid Mech. **519**, 55 (2004).
[14] L. Hsu, W. E. Dietrich, and L. S. Sklar, J. Geophys. Res. **113**, F02001 (2008).
[15] L. S. Sklar and W. E. Dietrich, Water Resour. Res. **40**, W06301 (2004).
[16] J. G. A. Bitter, Wear **6**, 169 (1963).
[17] I. Finnie, Wear **3**, 87 (1960).
[18] H. C. Meng and K. C. Ludema, Wear **181–183**, 443 (1995).

[19] J. F. Archard, J. Appl. Phys. **24**, 981 (1953).
[20] R. Artoni, A. Santomaso, and P. Canu, Phys. Rev. E **79**, 031304 (2009).
[21] N. Fillot, I. Iordanoff, and Y. Berthier, Tribol. Int. **40**, 973 (2007).
[22] L. S. Sklar and W. E. Dietrich, Geology **29**, 1087 (2001).
[23] L. Bocquet, É. Charlaix, and F. Restagno, C. R. Phys. **3**, 207 (2002).
[24] Ch. D. Willet, M. J. Adams, S. A. Johnson, and J. P. K. Seville, Langmuir **16**, 9396 (2000).
[25] GDR MiDi, Eur. Phys. J. E **14**, 341 (2004).
[26] B. Yohannes, L. Hsu, W. E. Dietrich, and K. M. Hill, J. Geophys. Res. **117**, F02027 (2012).
[27] E. Gardel, E. Keene, S. Dragulin, N. Easwar, and N. Menon, arXiv:cond-mat/0601022.
[28] S. N. Coppersmith, C.-h. Liu, S. Majumdar, O. Narayan, and T. A. Witten, Phys. Rev. E **53**, 4673 (1996).
[29] B. Miller, C. O'Hern, and R. Behringer, Phys. Rev. Lett. **77**, 3110 (1996).
[30] D. M. Mueth, H. M. Jaeger, and S. R. Nagel, Phys. Rev. E **57**, 3164 (1998).
[31] E. Longhi, N. Easwar, and N. Menon, Phys. Rev. Lett. **89**, 045501 (2002).
[32] R. Artoni, A. C. Santomaso, M. Go, and P. Canu, Phys. Rev. Lett. **108**, 238002 (2012).
[33] O. Pouliquen and Y. Forterre, Philos. Trans. R. Soc., A **367**, 5091 (2009).
[34] A. H. Clark, L. Kondic, and R. P. Behringer, Phys. Rev. Lett. **109**, 238302 (2012).